Annual and Interannual Behavior of Solar Ultraviolet Irradiance Revealed by Broadband Measurements[¶]

John E. Frederick*[1], James R. Slusser[2] and David S. Bigelow[2]

[1]Department of the Geophysical Sciences, The University of Chicago, Chicago, IL and
[2]Natural Resource Ecology Laboratory, Colorado State University, Fort Collins, CO

ABSTRACT

This research examines the behavior of ground-level solar UV radiation as measured by eight broadband meters in the continental United States during the period from late 1994 to late 1998. The goal is to define the variability that occurs in UV irradiance over time scales ranging from one to several years. The monthly integrated irradiances, from latitude 32°N to 47°N, contain large annual cycles and latitudinal gradients which depend on season. Seven of the eight sites show a maximum in July, a behavior related to proximity to the summer solstice, with modifications associated with the annual cycle in column ozone. A large interannual variability in monthly integrated irradiance appears over the 4 year period studied. A comparison of corresponding months during different years shows differences in irradiance of 20% or more in one-third of the cases analyzed. When the solar zenith angle (SZA) is held fixed in the range 60–65°, a substantial annual cycle in UV irradiance remains where the maximum monthly mean irradiance is 1.4–1.9 times the minimum, depending on location. Furthermore, the annual cycle at fixed SZA is not in phase with the normal seasonal cycle. Maximum irradiances at fixed SZA tend to occur in the October to December period, while minima cluster in April through July. The annual cycle in ozone, with maximum column values in spring and minima in autumn, explains the general character of the fixed-SZA data, although changes in cloudiness are significant contributors to interannual variability.

INTRODUCTION

Solar UV radiation at or near the Earth's surface drives air chemistry in clean and polluted environments (1), in addition to being a contributor to a variety of negative biological effects (2–4). The variation of ground-level UV irradiance with local time, latitude and season arises primarily from the changing path length taken by sunlight through an absorbing and scattering atmosphere as solar elevation varies over time scales ranging from hours to 1 year. Finally, changing optical properties of the local atmosphere, including ozone abundance, clouds, haze and particulates lead to additional variations in UV irradiance at a fixed site. These localized effects can be major factors in determining the radiation doses received by local biota and the vigor of chemical processes in a particular geographic region, such as an urban area.

This research examines the behavior of ground-level solar UV radiation measured from several locations during a 4 year period of the 1990s. Although considerable attention has focused on systematic changes in UV radiation in association with long-term trends in the ozone layer (5), it is apparent that regional meteorological conditions can lead to a large variability over a variety of time scales (6,7). This work seeks to define the variability that takes place in UV irradiance over time periods ranging from months up to several years. The objectives are (1) to define the nature and magnitude of interannual variability; (2) to examine the dependence of UV irradiance on location; and (3) to define the magnitude and character of the annual cycle in UV irradiance when the solar zenith angle (SZA)† is held fixed. This final objective addresses the role of atmospheric composition in driving an annual cycle in UV irradiance at the ground, when the large influence of a changing solar elevation is absent.

MATERIALS AND METHODS

Broadband meters. The data sets used in this research come from several broadband UV sensors operating in the continental United States as part of the United States Department of Agriculture (USDA) UV-B Monitoring Program (8). These meters have the advantages of mechanical simplicity and a high measurement frequency, and the resulting data set allows detailed studies of the temporal behavior in UV irradiance. The limitation is that the broadband information alone does not allow unambiguous attribution of observed variability to a specific cause, such as a change in ozone or in cloudiness.

The USDA program includes UVB-1 pyranometers manufactured by Yankee Environmental Systems (YES). In interpreting the data provided by these sensors, it is important to understand the relation-

---

*To whom correspondence should be addressed at: Department of the Geophysical Sciences, The University of Chicago, 5734 South Ellis Ave., Chicago, IL 60637, USA. Fax: 773-702-9505; e-mail: frederic@rainbow.uchicago.edu

†*Abbreviations:* CUCF, Central UV Calibration Facility; DU, Dobson unit; SRF, spectral response function; SZA, solar zenith angle; USDA, United States Department of Agriculture; YES, Yankee Environmental Systems.
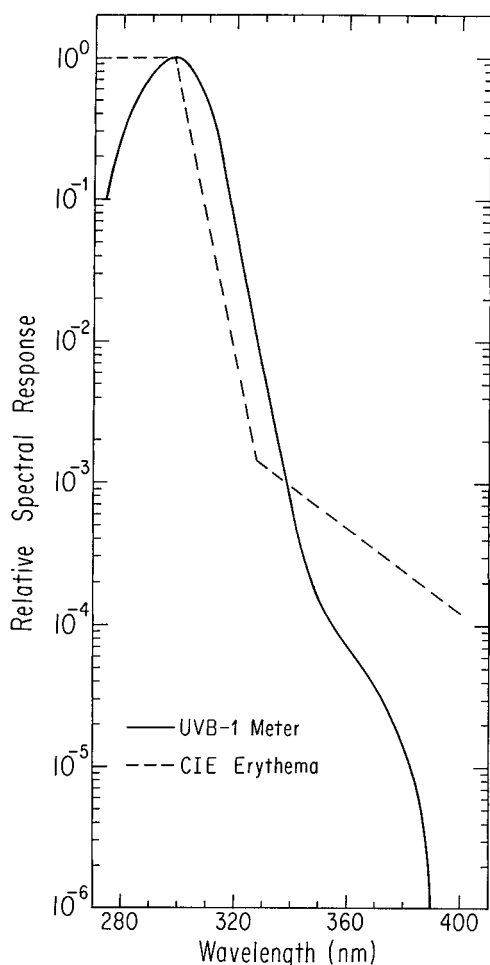
Figure 1. Typical spectral response function of the UVB-1 broadband meter and the action spectrum for erythema.

ship between their output and the incident solar radiation field. The spectral irradiance, $dE(\lambda)/d\lambda$ in watts per square meter of horizontal area per nanometer of wavelength expressed as a function of wavelength λ, is a standard descriptor of the solar radiation field. A spectroradiometer with high spectral resolution could measure $dE(\lambda)/d\lambda$ directly, but a broadband meter responds to a weighted integral of this quantity over wavelength. The output of the UVB-1 meters, E, is related to the solar spectral irradiance by:

$$E = \int d\lambda R(\lambda) \, dE(\lambda)/d\lambda \qquad (1)$$

where $R(\lambda)$ is the spectral response function of the meter. The integral in (Eq. 1) determines the sensitivity of a meter's output to changes in ozone amount, SZA and other atmospheric optical properties (9,10). Although the integral strictly extends over all wavelengths from zero to infinity, in practice both $R(\lambda)$ and $dE(\lambda)/d\lambda$ are nonzero only in the spectral region from approximately 290 to 390 nm. The short wavelength limit is set by $dE(\lambda)/d\lambda$ approaching zero as a consequence of strong absorption by atmospheric ozone, while the long wavelength limit is determined by the rapid decline in $R(\lambda)$ as λ increases. Figure 1 shows the typical wavelength dependence of the spectral response function, where the quantity has been normalized to 1.0 at its maximum. The sensitivity drops by a factor of 10^6 as wavelength increases from 300 to 390 nm. For practical purposes, wavelengths longer than 390 nm do not make a significant contribution to the output of the sensor. Comparison between different meters is predicated on their spectral response functions being very similar, an assumption which is valid (8).

If $R(\lambda)$ was proportional to the action spectrum for erythema, also shown in Fig. 1 (11), then the output of the meters would be equivalent to the erythemal irradiance. Figure 1 shows that this equality is not strictly true, although the UVB-1 measurements provide a reasonable proxy for erythemal irradiance. A logical choice is for $R(\lambda)$ to be unitless, so that E has the units of irradiance, watts per square meter of horizontal area. In general one can write:

$$R(\lambda) = R_0 \, f(\lambda) \qquad (2)$$

where R_0 is a constant with the units of wavelength, and $f(\lambda)$ is normalized such that:

$$\int d\lambda f(\lambda) = 1 \qquad (3)$$

and the integral extends from zero to infinity. Note that $f(\lambda)$ has the units of inverse wavelength. The structure of the meter determines $f(\lambda)$, while the convention adopted in the calibration fixes the value of R_0. For the UVB-1 meters, R_0 is chosen such that the daily maximum irradiance at local noon in summer for a clear middle latitude location is typically near 4 W m^{-2}.

Biases and uncertainties in measured irradiances. Possible biases and uncertainties in the broadband measurements may be divided into three areas: angular or cosine response, radiometric sensitivity or gain and the spectral response function (SRF). Any of these factors could vary in a single instrument over the time period between successive calibrations. There could also be instrument-to-instrument differences that influence the data set at a fixed location since a new detector is placed at each site as part of the yearly calibration process. The following paragraphs summarize the calibration procedure, followed by estimates of systematic biases and random errors in the measured irradiances.

The first USDA broadband measurements began in October 1993. As of December 1994, the starting data for data considered in this paper, six sites were reporting UV data. Calibrations of all of the USDA broadband sensors were handled by YES until 1998 (8) and by the Central UV Calibration Facility (CUCF) at the National Oceanic and Atmospheric Administration in Boulder, CO, beginning in October 1997 (9). During 1997 and 1998 twelve UVB-1 sensors were calibrated by both YES and CUCF. The instruments were swapped out for annual calibrations, so every year a different detector resided at each site.

The calibration procedure included spectral and absolute response characterizations. The absolute calibration was performed by comparing the output of the broadband sensor in sunlight with that of a collocated UVB-1 standard instrument. This standard had itself been calibrated on 27 January 1993 by Dr. Richard McKenzie in Lauder, New Zealand using a spectroradiometer (12). The calibration transfer is accurate to 1%, and the calibration factor obtained was 1.97 V W^{-1} m^2. In all subsequent calibrations, YES adjusted the gain of each UVB-1 so as to normalize its daily irradiance integral to that of the standard. To verify the stability of the standard UVB-1, Dr. McKenzie performed another spectroradiometer-based calibration of the UVB-1 standard instrument on 15 March 1999. The calibration factor obtained here was 2.03 V W^{-1} m^2, only 3% higher than the value determined 6 years earlier.

Tests carried out by CUCF in conjunction with radiative transfer calculations allow one to estimate systematic biases in measured irradiances associated with an imperfect cosine response of the UVB-1. This issue is most important under clear skies where the direct component of solar irradiance on a horizontal surface makes the maximum contribution to the total irradiance. The angular response of the sensors was measured in two orthogonal planes at CUCF. This information was combined with direct and diffuse irradiances computed from a radiative transfer code (13) assuming a hemispherically isotropic scattered radiation field. Errors introduced by the assumption of hemispheric isotropy are estimated to be less than 4% (14–16). We computed the ratio of direct to total horizontal irradiance as a function of SZA and column ozone amount. This ratio changed by less than 1% as column ozone varied by 50 Dobson units (DU), about 300 DU, so for subsequent calculations we used only the ratios computed for the central ozone value.

We then used the angular response corrections from CUCF with the computed direct-to-total irradiance ratios to correct a sample of
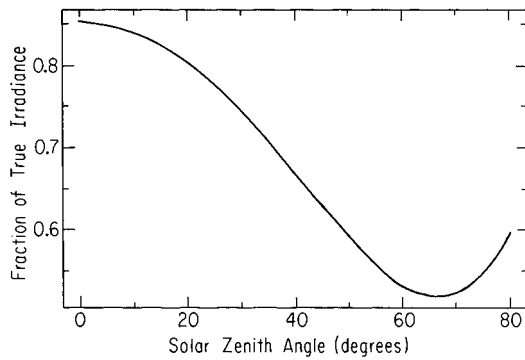
Figure 2. Angular response correction as a function of SZA. The vertical scale is the ratio of measured irradiance to true irradiance, where the latter includes the angular response correction measured by CUCF. The irradiances include both the direct and diffuse components.

the broadband irradiances for the imperfect cosine response. Figure 2 presents the ratio of the measured irradiance, with no corrections, to the irradiance that includes cosine corrections as a function of SZA. When the angular correction is not applied, the measured irradiances lie between 55 and 90% of the true irradiance, depending on SZA. For the analyses performed in this paper differences in cosine response from instrument-to-instrument are more relevant than the absolute bias in Fig. 2. The angular responses of 10 different UVB-1 sensors were measured at the National Institute for Standards Technology, and this revealed virtually identical results, with a variability of less than 0.1% (8).

A single UVB-1 sensor in the field can experience a change in overall radiometric sensitivity or gain during the year between successive calibrations. The approximate 3% change in the UVB-1 standard instrument between 1993 and 1999 corresponds to a drift of about 0.5% per year, although this could be due to changes both in sensitivity and in the SRF. To be conservative and potentially overestimate the error, we assign an uncertainty of 1% per year to the possible sensitivity change experienced by detectors operating in the field. Another issue centers on differences in sensitivity between sensors that are swapped at a fixed site as part of the annual calibration procedure. If a single sensor is stable to better than 1% during 1 year of operation and each sensor is forced to agree to within 1% of the standard instrument each year, then the swapping of sensors will introduce a random uncertainty of less than 2%. These values are in general agreement with independent observations of an earlier generation of broadband meter after extended field use (17).

Estimates of the uncertainty associated with changes in the SRF are obtained in a manner analogous to that for the radiometric sensitivity. We make a conservative estimate of a 1% per year uncertainty due to changes in the SRF of a single UVB-1 sensor in the field. The annual instrument swap, using a replacement UVB-1 which agrees to within 1% of the standard, will lead to a total uncertainty of less than 2%.

An overall uncertainty budget for the USDA UVB-1 sensors must combine the factors identified above. Note that the imperfect cosine response represents a systematic bias, while uncertainties associated with radiometric sensitivity and the SRF are random. Based on estimated errors of up to 2% each due to radiometric sensitivity and SRF, we assign a random error of ±3% to the measured irradiances. The atmospheric variability observed by the UVB-1 sensors is much larger than these uncertainties.

Data sets. We selected eight stations from the USDA network for analysis. Table 1 lists the stations, their latitudes, longitudes, elevations above sea level and the time periods for which data are studied. Henceforth, we identify each station by the abbreviation for the state in which it is located. The stations span the range of latitude and elevation found in the continental United States. We consider data sorted according to calendar month and, in some cases, according to season, where ''winter'' is defined as December through February, and ''summer'' is June through August, consistent with the usage of Trenberth (18). We used all data available from December 1994 through November 1998. The analysis considers ''1 year'' as beginning in December and extending through the following November. This definition was made so that a complete winter season (December 1994 through February 1995) was available at the beginning of the period of study. Similarly, the data sets end with a complete autumn season. Data sets from six of the eight sites in Table 1 (NM, GA, CA, CO, IL and WA) were essentially complete from December 1994 through November 1998, the exception being two missing months from 1998 at the IL site. Data from the ME site began in November 1995 and were continuous thereafter, while the earliest data from the MD site were for March 1997.

Each UVB-1 meter produces one irradiance measurement every 3 min, and this comprehensive body of information allows for studies of a type that have not been possible in the past. For example, one can compute irradiances integrated over time, such as monthly integrals, knowing that all but the highest frequency variability in the radiation field has been included in the result. In addition, from the database one can extract only those measurements made in a narrow range of SZA. When the large variations in UV irradiance associated with the changing SZA are removed, the effects due to changes in atmospheric optical properties are readily observed. This type of study is feasible only because of the high frequency with which data are acquired.

RESULTS AND DISCUSSION

Monthly integrated irradiances

We used the data set from each site to compute monthly integrated irradiances and from these produced multiyear averages based on the time periods listed in Table 1. Figure 3 presents the results, for which a convenient unit is 10^5 J m^{-2}.

Table 1. Locations of USDA UVB-1 sensors used in this research

Location	Designation	Latitude (°N)	Longitude (°E)	Elevation (m*)	Time period
Jornada, New Mexico	NM	32.62	106.74	1317	Dec 1994–Nov 1998
Griffith, Georgia	GA	33.18	84.41	270	Dec 1994–Nov 1998
Davis, California	CA	38.53	121.76	18	Dec 1994–Nov 1998
Wye, Maryland	MD	38.92	76.17	7	Mar 1997–Nov 1998
Bondville, Illinois†	IL	40.05	88.37	213	Dec 1994–Nov 1998
Nunn, Colorado‡	CO	40.79	104.76	1641	Dec 1994–Nov 1998
Presque Isle, Maine	ME	46.68	68.04	144	Nov 1995–Nov 1998
Pullman, Washington	WA	46.75	117.18	804	Dec 1994–Nov 1998

* Elevation above sea level.
† April and June of 1998 are missing.
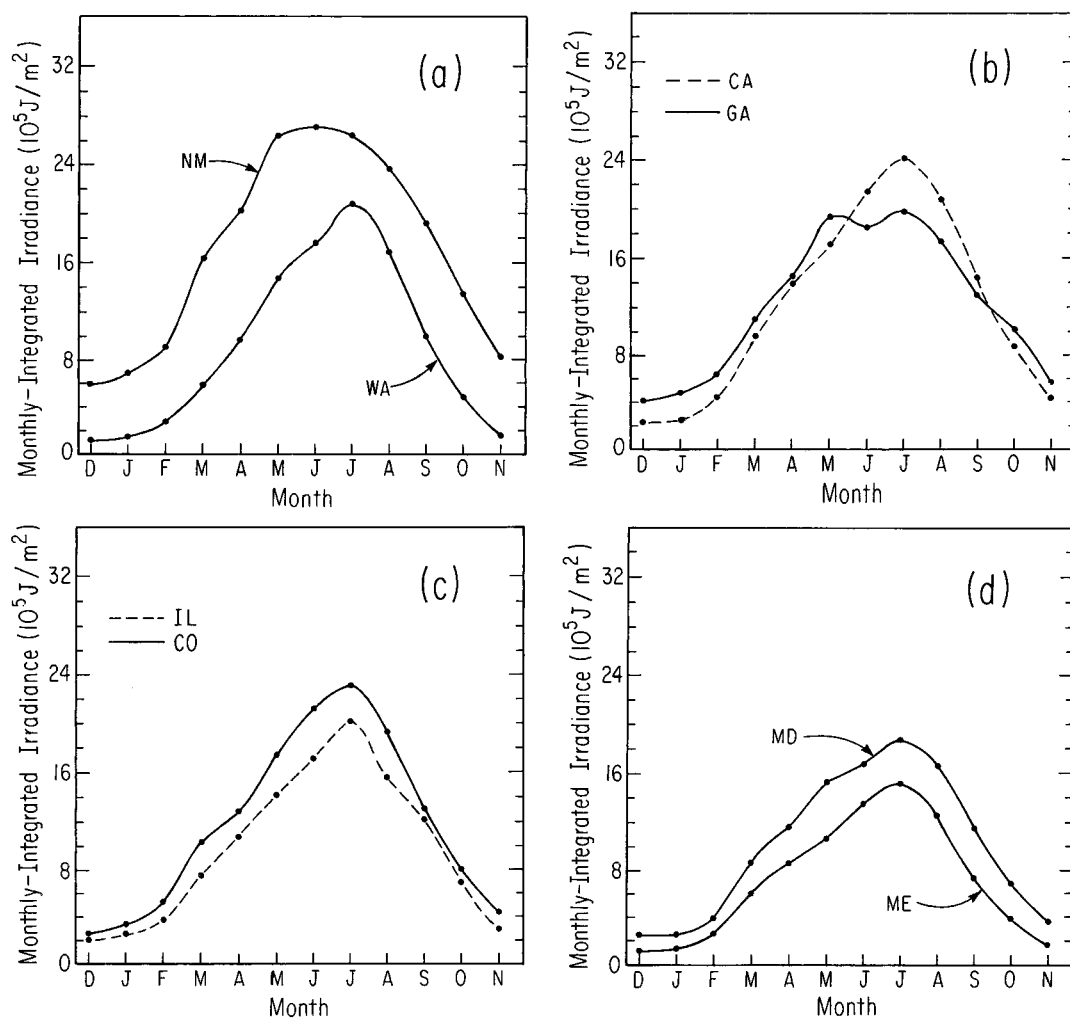‡ Rual site on USDA's Central Plains Experimental Range.

Figure 3. Annual cycle in monthly integrated solar irradiance based on measurements from UVB-1 pyranometers at the sites indicated: (a) NM and WA, (b) GA and CA, (c) IL and CO and (d) MD and ME.

The systematic variation in SZA over a year is the dominant factor that determines the nature of the annual cycle, although as noted below, other variables enter as well. Since the values in Fig. 3 are integrals from sunrise to sunset for each day of month-long periods, the irradiances include the effects of a changing SZA at a fixed local time over a year as well as the changing duration of daylight. These two influences combine to produce an annual cycle whose amplitude is larger than one would expect from observing the behavior at a fixed time such as local noon. The sites at NM and WA (Fig. 3a) represent the extremes of latitude studied here as well as differing elevations. As expected, UV irradiance increases as one moves south and to higher elevations, while the amplitude of the annual cycle decreases on a percentage basis. The ratio of integrated irradiance in the month of summer maximum to the month of winter minimum is 4.6 at NM, and the corresponding ratio for WA is 16.6.

If SZA were the only variable that influenced the annual cycle, then irradiances would be symmetrical around the summer solstice near 21 June, with the result that June would be the time of largest monthly integrated irradiance. Yet, inspection of Fig. 3 shows that July has the maximum integrated irradiance at seven of the eight sites. The exception is NM where a broad maximum from May through July exists, with the largest values occurring in June. The fact that July has 31 days as opposed to 30 days for June leads to the former month having the longer daylight period. If we define T(day) as the number of seconds per month when the SZA is less than 90°, then T(day) for July exceeds that in June by about 1.8% for NM and 1.6% for WA. Note that these values are smaller than the expected 3.3% difference, due solely to the differing number of days in the 2 months. This effect arises from the shortening day length throughout July.

The annual cycle in column ozone is a more important contributor to the July maxima in Fig. 3. Maximum column amounts occur in late winter or early spring, followed by a decline to a minimum, typically in October (5). During the months May through August when the SZA promotes large UV irradiances, the column ozone amount is declining. This effectively pushes the time of maximum radiation levels from June into July at most locations, although lower latitude sites are more likely to be exceptions. The annual cycle in ozone also introduces an asymmetry into the annual cycle in UV irradiance, where irradiances near the autumn equi-
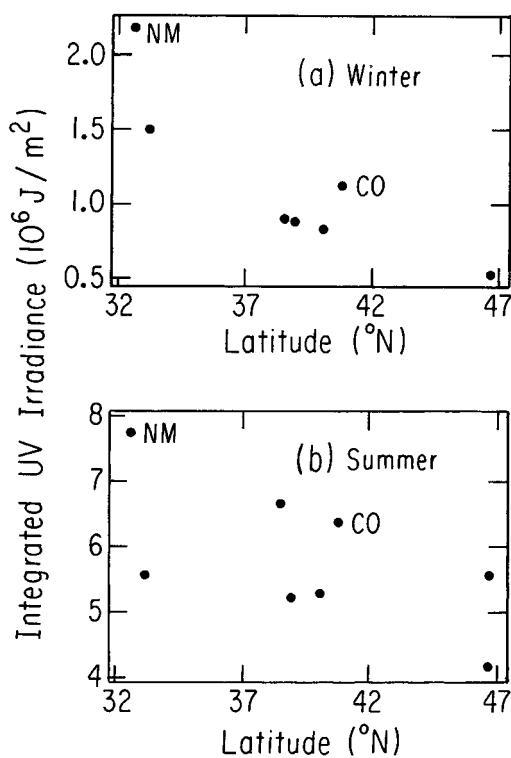
Figure 4. (a) Seasonally integrated UV irradiance for winter (December, January, February) as a function of latitude for each UVB-1 site. The two points that lie above the rest refer to the highest elevation sites, NM (32.62°N) and CO (40.79°N). The points are based on all years of data listed in Table 1. (b) Seasonally integrated UV irradiance for summer (June, July, August) *versus* latitude.

nox, a time of low ozone amounts, exceed those near the spring equinox.

The role of cloudiness and haze as modulators of UV irradiance cannot be quantified from Fig. 3 alone. However, some of the structure in the plots surely arises from clouds. The most obvious example of this is at the GA site (Fig. 3b) where a local minimum in UV irradiance occurs in June. Also, from the latitude separation between the CA and GA sites, one would expect the GA curve to lie above that for CA in all months, but the difference between the two locations from June through September is contrary to these expectations. This fact, combined with the local minimum in June at GA, suggests a large influence of cloudiness or restricted visibility at this site, an inference consistent with cloud climatologies (19).

During winter the SZA increases and the day length decreases as one moves north. Both of these effects promote smaller irradiances at higher latitudes. Figure 4a presents the seasonally integrated wintertime irradiances, being the sum of monthly integrals for December, January and February, plotted against the latitude of each site. Near 47°N the points for WA and ME are nearly indistinguishable. The values for CO and NM are relatively high, but a smooth curve whose slope increases with decreasing latitude fits the remaining six points. A regression model of the form $\ln E = a_0 + a_1 \cos \theta + a_2 Z$, where E is the seasonally integrated irradiance, θ is the latitude and Z is the elevation of the observing site above sea level, explains 98.4% of the variance in the spe-

cific data sets analyzed here. The situation for summer, shown in Fig. 4b, is more complicated than that in winter. Here day length increases northward and opposes the increasing SZA as an influence on seasonally integrated UV irradiance. Overall there is a tendency for the integrated irradiance to decrease as latitude increases, but the scatter among sites is large. For example, the summertime integrals for GA (33.18°N) and WA (46.75°N) are essentially identical despite their latitude separation. The regression model used above explains only 68.8% of the variance in this case. The fact that much of the summertime variance remains unexplained implies that factors unique to each location, most likely local cloudiness and visibility, are important determinants of site-to-site differences in UV irradiance at this time of year.

Interannual variability

The magnitude of interannual variability in UV irradiance is important both as it relates to short-term health effects, such as sunburn, and to the photochemical production of secondary air pollutants. With at most 4 years of irradiances at each site, the duration of the data record does not warrant a rigorous statistical evaluation. Instead we characterize interannual variability in the following two ways. Let $E(s, m, y)$ be the monthly integrated irradiance at site ''s'' for month ''m'' of year ''y'', and $\langle E(s, m) \rangle$ be the corresponding multiyear average over all y for the site and calendar month as shown in Fig. 3. The ''irradiance spread'' for site s and month m is defined as:

$$S(s, m) = E(s, m, y_{max}) - E(s, m, y_{min}) \qquad (4)$$

in J m^{-2} where y_{max} is the year of the largest irradiance in the data set and y_{min} is the year of the smallest irradiance. Since the integrated irradiances contain a large annual cycle, one might expect similar behavior in $S(s, m)$. Another useful measure of interannual variability is the ''percent range'' defined as:

$$R(s, m) = 100 S(s, m) / \langle E(s, m) \rangle \qquad (5)$$

Since the annual cycle associated with the SZA is removed from $R(s, m)$, the percent range measures interannual variability in the optical properties of the local atmosphere. Figure 5, for IL, illustrates typical values of the monthly irradiance spreads (upper panel) and percent ranges (lower panel), where the latter is a particularly useful measure of interannual variability. The entire data set of all eight sites contains 93 months of information. In 69 of these months the percentage range exceeds 10%, and it equals or exceeds 20% in 31 months. Although there are differences in detail from site to site, there is a tendency for small percentage variability to appear in summer and to persist into September or, in some cases, October.

Figure 6 compiles information from all eight sites so as to reveal systematic behavior over the annual cycle. Specifically, Fig. 6 indicates the timing of (1) the maximum percent range; (2) the maximum absolute spread; and (3) the maximum monthly integrated irradiance by plotting the number of sites experiencing the associated maximum in each calendar month. The figure is based on only seven stations since MD has less than 2 full years of data. The top
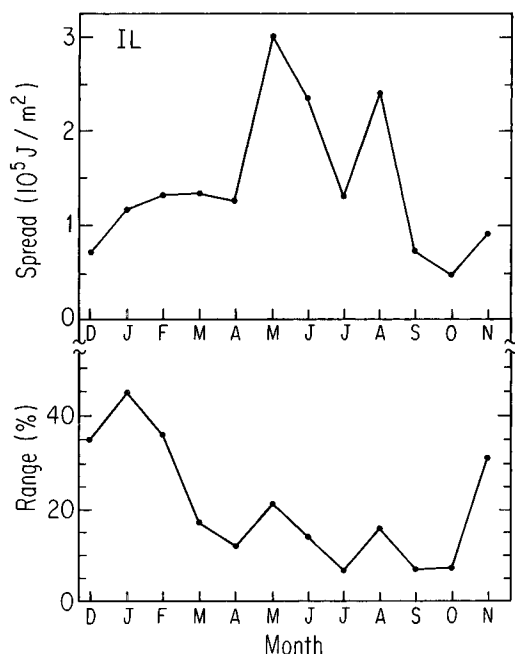
Figure 5. Interannual variability in monthly integrated UV irradiance for IL. The top panel gives the spread in absolute irradiance between the maximum and minimum measured values. The bottom panel indicates the range between maximum and minimum expressed as a percent of the multiyear average monthly integrated irradiance.

Figure 6. Months in which (a) the maximum percentage interannual variability in irradiance occurs, (b) the maximum absolute interannual variability in irradiance occurs and (c) the maximum monthly integrated irradiance occurs. Vertical lines indicate the number of sites that experience the associated maximum in each month.

panel of Fig. 6 reveals that the maximum percent ranges avoid the summer period and occur with no clear preference as to month during the remainder of the year from October through May. This shows that atmospheric optical properties in the summer, the time of largest absolute irradiance, tend to be more repeatable from year to year than in other months, although Fig. 6 indicates that the summertime variability is still substantial. Comparison of the center and bottom panels of Fig. 6 demonstrates the tendency for the maximum absolute spread in irradiance to occur earlier in the year than the maximum irradiances themselves. Four of the seven stations experience the maximum spread in May, a behavior which would arise if atmospheric optical properties show more interannual variability in spring than in summer.

Irradiances at constant SZA

If the optical characteristics of the atmosphere (ozone, cloudiness, visibility) remained constant throughout the year, then the varying SZA and changes in the duration of daylight would be the only mechanisms for variability in UV irradiance. Changes in SZA are, in fact, the dominant driver of the annual cycles evident in Fig. 3. However, the high time resolution of the UVB-1 measurements provides for an analysis of irradiances at essentially constant SZA throughout the multiyear duration of the data set, thereby allowing us to isolate the influence of variations in atmospheric optical properties.

We scanned the entire data set from each site in Table 1 and extracted all irradiances recorded at SZA between 60 and 65°. This range of SZA was selected because it occurs at all eight sites throughout the year, with minor exceptions.
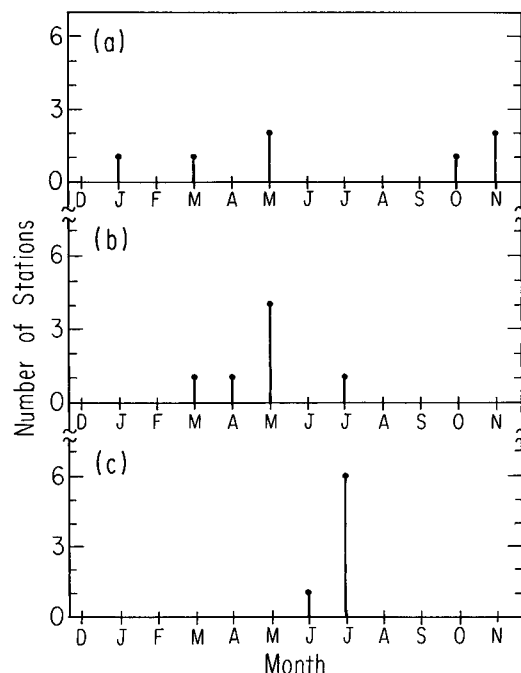
These exceptions are the two highest latitude sites, ME and WA, in December. In addition, for ME and WA during January SZA between 60 and 65° were infrequent compared to other months, and they tended to cluster near the large side of the SZA bin rather than being evenly distributed over the 5° interval. We therefore chose to eliminate January at ME and WA as well. We then sorted the irradiances into time intervals 1 month long. The number of measurements in a 5° wide SZA bin varied by site and month of the year. A typical number is 500–600 points per month, although the values ranges from a low of 232 points to a maximum in excess of 1500 points. The exact number depends on the length of time the sun occupies the 60–65° SZA range in a given month, and this varies over the course of the year.

The simplest approach would be to compute the average value of UV irradiance for each site and month based on all measurements made between SZA of 60 and 65°. However, some of the variability among irradiances in a 5° wide bin is due to the variation of the SZA itself. Although this is a small effect compared to changes in the optical properties of the atmosphere, we chose to correct for it. To do this we performed a linear fit of the form $E(\zeta) = b_0 + b_1 \cos \zeta$ to the data points in a fixed month where ζ is the SZA, always in the range 60–65°. We then used the resulting ζ-dependence to adjust each measured irradiance so that it refers to a SZA of 62.5°. In practice this was a very small correction. In two significant figures, the adjustment did not alter the average irradiance computed for a full month of data, but the adjustment did reduce the standard deviation.

Figure 7 presents the behavior of the fixed-SZA UV irradiances for the duration of the data set at each site, where the horizontal scales are ''month number'' where ''1'' refers
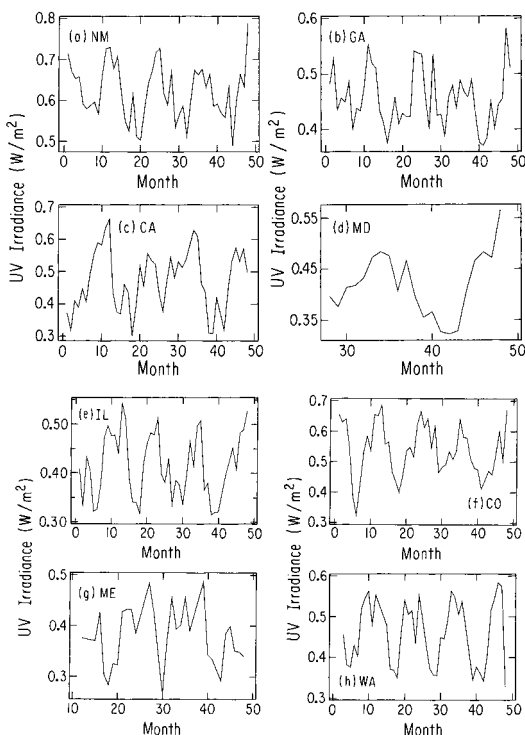
Figure 7. Temporal behavior of UV irradiance at a fixed SZA. The values are monthly averages of all irradiances measured at SZA between 60 and 65°. The horizontal scale labels the month, where month number 1 is December 1994, and month number 48 is November 1998: (a) NM, (b) GA, (c) CA, (d) MD, (e) IL, (f) CO, (g) ME and (h) WA.

to December 1994 and ''48'' is November 1998. The values plotted are the monthly averaged irradiances at fixed SZA, where lines are included to allow easy visualization of systematic behavior. The variations arise from changing atmospheric optical characteristics, the most important of these being ozone and cloudiness, although effects of a changing surface albedo from summer to winter (20) and the varying Earth–sun distance will contribute as well. Each site reveals an annual cycle, although it is not in phase with the widely recognized annual cycle associated with variations in SZA. Maximum monthly averaged irradiances appear in various months ranging from August through March, but never in June or July. The ratio of maximum fixed-SZA irradiance to the minimum value in a year is typically in the range 1.4–1.9. While of significant size, this is much smaller than the amplitudes of the annual cycles related to the changing SZA in Fig. 3.

Figure 8 indicates the months in which (1) the maximum; and (2) the minimum fixed-SZA irradiances occur based on all useable stations and years. Two locations, WA and ME, are omitted from Fig. 8a because of the missing or sparse information in December and January. Of a total of 21 site-years, where 1 ''site-year'' means 1 full year of data at one site, 20 of the annual maxima occur in the period August through January, with the remaining one in March. Figure 8b, the months in which the minimum fixed-SZA irradiances occur, includes data from ME and WA, giving a total of 28 site-years. There is a tendency for the smallest irradiance to occur in April and May, a total of 15 site-years. In general,
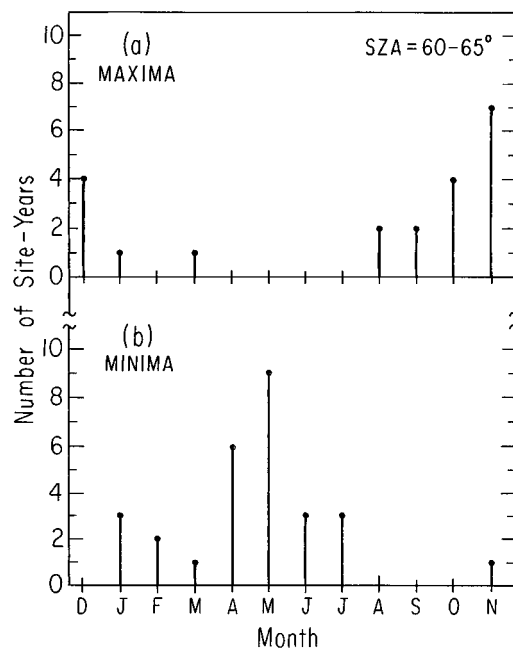

Figure 8. Months in which the extreme values of UV irradiance at fixed SZA (60–65°) occur. The vertical lines indicate the number of site-months that experience the extreme at the time indicated on the horizontal scale. (a) Months of maximum UV irradiance at fixed SZA. (b) Months of minimum UV irradiance at fixed SZA.

all but one minimum occurs in the period January through July.

Two quantities that vary with annual cycles and influence UV irradiance at the ground are the extraterrestrial solar irradiance and the atmospheric column ozone amount. The elliptical nature of the Earth's orbit leads to a repeatable annual cycle in UV irradiance at the top of the atmosphere. The amplitude of this cycle, where the maximum exceeds the minimum by a factor of 1.06–1.07, is substantially less than the amplitude displayed by the fixed-SZA UV irradiance, although it is not negligible. Since the extraterrestrial variation is well known, we can remove it from the monthly averaged fixed-SZA irradiances. The annual cycle that remains in the adjusted irradiances must be associated with the behavior of atmospheric optical properties.

It is possible to demonstrate a relationship between the annual cycles in fixed-SZA irradiances and in column ozone using archived measurements from the Total Ozone Mapping Spectrometer on the Nimbus 7 satellite (21). Since the focus here is on the general character of the annual cycle, it is not necessary to use ozone data coincident in time and space with the ground-based sensors. To obtain a representative annual cycle, we averaged the ozone data over a 5 year period, December 1985 through November 1990, at latitudes appropriate for comparison with the UVB-1 sites. Figure 9 shows the monthly fixed-SZA UV irradiances plotted against column ozone, where all eight sites are included. The plotted irradiances have been corrected for the varying Earth–sun distance over a year and for the differing elevations of the measurement sites using the regression model identified earlier in this section. The scatter arises from the fact that the ozone values are not simultaneous in time and space with the irradiances and, probably more important,
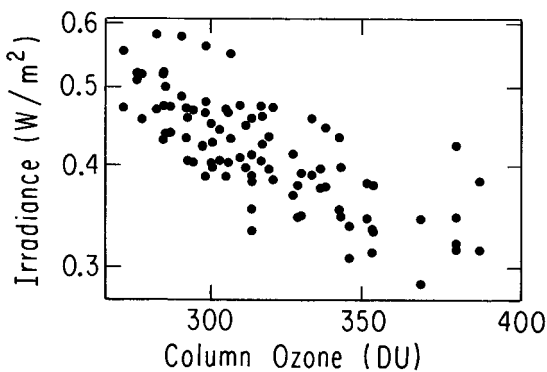
Figure 9. Relationship between monthly averaged UV irradiance measured at a fixed SZA (60–65°) and column ozone. Column ozone explains 72.5% of the variance in irradiance after correction for the varying Earth–sun distance and the differing elevations of the measurement sites.

that cloudiness varies from one site to another as well as with month and year. Still, the overall character of the annual cycle in column ozone is consistent with the annual cycle in UV irradiance at fixed SZA and explains 72.5% of the variance.

CONCLUSIONS

The variation of ground-level UV irradiance with latitude, season and elevation revealed by the broadband meters is broadly consistent with theoretical expectations. The large annual cycle in monthly integrated broadband UV irradiance usually has a peak in July, although the maximum shifts to June at the lower latitudes studied here. During summer, the lengthening duration of daylight with latitude, as one approaches the pole, counteracts the increase in SZA at a fixed local time, thereby providing a weaker latitudinal gradient in UV irradiance than at other times of the year. Under this circumstance, localized atmospheric conditions such as cloudiness and limited visibility can have a substantial influence on the differences in radiation levels between sites. The USDA sites in GA and WA are prime examples of this. The summertime-integrated UV irradiances at these two locations are virtually identical despite a 13–14° separation in latitude.

Irradiances measured in the range of SZA from 60–65° reveal an annual cycle which is not in phase with that associated with the changing Earth–sun geometry. Maximum fixed-SZA irradiances cluster in the October through December time frame, with minima most frequent from April through July. The maxima exceed the minima by factors of 1.4–1.9 depending on location. The annual cycle in column ozone explains the overall character of the annual behavior at fixed SZA.

Interannual variability in UV irradiance arises from an interplay of variations in cloudiness and column ozone meshed with the regular cycles in SZA. Comparison of monthly integrated broadband irradiances from corresponding months of various years reveals differences in excess of 10% in most cases, and differences that exceed 20% in one-third of the months studied. The smallest percentage variability tends to occur in summer, while maxima in variability are distributed over a range of months in the remaining three seasons. Although the broadband meters alone cannot un-

ambiguously identify the cause of this variability, the large magnitude appears consistent only with changing cloudiness. Since cloudiness over a region can change in an erratic way from one year to the next, large interannual fluctuations, as opposed to systematic trends, will likely be the dominant form of variability in broadband UV irradiance in a long-term database at middle latitudes.

REFERENCES

1. Tang, X., S. Madronich, T. Wallington and D. Calamari (1998) Changes in tropospheric composition and air quality. *J. Photochem. Photobiol. B: Biol.* **46**, 83–95.
2. Longstreth, J., F. R. de Gruijl, M. L. Kripke, S. Abseck, F. Arnold, H. I. Slaper, G. Velders, Y. Takizawa and J. C. van der Leun (1998) Health risks. *J. Photochem. Photobiol. B: Biol.* **46**, 20–39.
3. Caldwell, M. M., L. O. Bjorn, J. F. Bornman, S. D. Flint, G. Kulandaivelu, A. H. Teramura and M. Tevini (1999) Effects of increased solar ultraviolet radiation on terrestrial ecosystems. *J. Photochem. Photobiol. B: Biol.* **46**, 40–52.
4. Hader, D.-P., H. D. Kumar, R. D. Smith and R. C. Worrest (1998) Effects on aquatic ecosystems. *J. Photochem. Photobiol. B: Biol.* **46**, 53–68.
5. World Meteorological Organization(1999) *Scientific Assessment of Ozone Depletion: 1998,* Global Ozone Research and Monitoring Project—Report No. 44, Geneva.
6. Erlick, C., J. E. Frederick, V. K. Saxena and B. N. Wenny (1998) Atmospheric transmission in the ultraviolet and visible: aerosols in cloudy atmospheres. *J. Geophys. Res.* **103**, 31 541–31 556.
7. Frederick, J. E., Z. Qu and C. R. Booth (1998) Ultraviolet radiation at sites on the Antarctic coast. *Photochem. Photobiol.* **68**, 183–190.
8. Bigelow, D. S., J. R. Slusser, A. F. Beaubien and J. H. Gibson (1998) The USDA ultraviolet radiation monitoring program. *Bull. Am. Meteorol. Soc.* **79**, 601–615.
9. Lantz, K. O., P. Disterhoft, J. J. DeLuisi, E. Early, A. Thompson, D. Bigelow and J. Slusser (1999) Methodology for deriving clear-sky erythemal calibration factors for UV broadband radiometers of the Central UV Calibration Facility. *J. Atmos. Oceanic Technol.* **16**, 1736–1752.
10. Bodhaine, B., E. G. Dutton, R. L. McKenzie and P. V. Johnston (1998) Calibrating broadband UV instruments: ozone and solar zenith angle dependence. *J. Atmos. Oceanic Technol.* **15**, 916–926.
11. McKinlay, A. F. and B. L. Diffey (1987) A reference action spectrum for ultraviolet induced erythema in human skin. *CIE Res. Note* **6**, 17–22.
12. Grangier, R. G., R. E. Basher and R. L. McKenzie (1993) UV-B Robertson–Berger meter characterization and field calibration. *Appl. Opt.* **32**, 343–349.
13. Stamnes, K., S. Tsay, W. Wiscombe and K. Jayaweera (1988) Numerically stable algorithm for discrete ordinate-method radiative transfer in multiple scattering and emitting layered media. *Appl. Opt.* **27**, 2502–2509.
14. Grobner, J., M. Blumthaler and W. Ambach (1996) Experimental investigation of spectral global irradiance measurements errors due to non-ideal cosine response. *Geophys. Res. Lett.* **23**, 2493–2496.
15. Leszczynski, K., K. Jokela, L. Ylianttila, R. Visuri and M. Blumthaler (1997) *Report of the WMO/STUK Intercomparison of Erythemally-Weighted Solar UV Radiometers,* WMO/GAW Report Number 112, Geneva.
16. Leszczynski, K., K. Jokela, L. Ylianttila, R. Visuri and M. Blumthaler (1998) Erythemally weighted radiometers in solar

UV monitoring: results from the WMO/STUK intercomparison. *Photochem. Photobiol.* **67**, 212–221.

17. DeLuisi, J., J. Wendell and F. Kreiner (1992) An examination of the spectral response characteristics of seven Robertson–Berger meters after long-term field use. *Photochem. Photobiol.* **56**, 115–122.

18. Trenberth, K. E. (1983) What are the seasons? *Bull. Am. Meteorol. Soc.* **64**, 1276–1282.

19. Warren, S. G., C. J. Hahn, J. London, R. M. Chervin and R. L. Jenne (1986) *Global Distribution of Total Cloud Cover and Cloud Amount Over Land,* NCAR Technical Notes, NCAR/TN-273+STR, Boulder, CO.

20. Kerr, J. B. (1997) Observed dependencies of atmospheric UV radiation and trends. In *Solar Ultraviolet Radiation Modeling, Measurements, and Effects*, Vol. I (Edited by A. F. Bais and C. S. Zerefos), pp. 259–266. Springer-Verlag, Berlin.

21. McPeters, R. D., S. M. Hollandsworth, L. E. Flynn, J. R. Herman and C. J. Seftor (1996) Long-term ozone trends derived from the 16-year combined Nimbus 7/Meteor 3 TOMS Version 7 record. *Geophys. Res. Lett.* **23**, 3699–3702.